[Short title + Author Name - P&H title] 32 (2024) 101892

HOSTED BY

ELSEVIER

Contents lists available at ScienceDirect

Saudi Pharmaceutical Journal

journal homepage: www.sciencedirect.com

Pentagamavunone-1 inhibits aggressive breast cancer cell proliferation through mitotic catastrophe and ROS-mediated activities: *in vitro* and *in vivo* studies

Dhania Novitasari [a], Ikuko Nakamae [b], Riris Istighfari Jenie [a,c], Noriko Yoneda-Kato [b], Jun-ya Kato [b,*,1], Edy Meiyanto [a,c,*,1]

[a] *Cancer Chemoprevention Research Center, Faculty of Pharmacy, Universitas Gadjah Mada, Yogyakarta 55281, Indonesia*
[b] *Laboratory of Tumor Cell Biology, Division of Biological Science, Graduate School of Science and Technology, Nara Institute of Science and Technology, Nara 630-0192, Japan*
[c] *Department of Pharmaceutical Chemistry, Faculty of Pharmacy, Universitas Gadjah Mada, Yogyakarta 55281, Indonesia*

ARTICLE INFO

Keywords:
Curcumin analog
Mitotic arrest
ROS generation
Breast cancer

ABSTRACT

Pentagamavunone-1 (PGV-1), an analog of curcumin, has been studied for its cytotoxic effects in 4T1, MCF7, MCF7/HER2, and T47D breast cancer cells. Its antiproliferative effect is partly mediated through G2/M arrest; however, its molecular mechanism during cell cycle progression remains unknown. In this study, we aimed to determine whether PGV-1 has any anticancer effects on highly aggressive breast cancer cells, with a focus on cell cycle regulatory activity, reactive oxygen species (ROS) generation, and their mediated effects on cancer cells. MDA-MB-231 (triple-negative) and HCC1954 (overexpressed HER2) immortalized human breast cancer cells were used in the study. PGV-1 exhibited cytotoxic activity with an irreversible antiproliferative impact on treated cells and had good selectivity when tested in fibroblast cells. Oral PGV-1 administration suppressed tumor growth in a cell-derived xenograft mouse model. PGV-1 induced the phosphorylation of Aurora A kinase and PLK1 in MDA-MB-231 cells, while PLK1 and cyclin B1 phosphorylation were enhanced in the PGV-1-treated HCC1954 cells during prometaphase arrest. Intracellular ROS production was substantially higher upon PGV-1 treatment following mitotic arrest, and this activity caused impairment of mitochondrial respiration, induced senescence, and subsequently triggered early-to-late apoptosis. Collectively, these results suggest that the molecular mechanism of PGV-1 involves the regulation of mitotic kinases to cause cell cycle arrest and the enhancement of ROS production to impair mitochondrial activity and induce cellular senescence. The therapeutic activities demonstrated by PGV-1 in this study show its potential as an appealing candidate for chemotherapy in breast cancer treatment.

1. Introduction

Breast cancer, the most common cancer in women worldwide, is commonly classified as either luminal, HER2-positive, or triple-negative breast cancer (TNBC) (Makanjuola et al., 2014). The triple-negative subtype constitutes approximately 15–20% of the total reported breast cancer cases (Damaskos et al., 2019), while cases characterized by the overexpression of the HER2 protein are observed in 20–30% of cases (Wahler and Suh, 2015). Both subtypes are notable for their aggressiveness due to high heterogeneity in metabolism (Willmann et al., 2015), cell cycle regulation (Lashen et al., 2021), and other clinical and histopathological aspects, which makes the treatment options complicated (Guo et al., 2023). Along with the available types of anticancer chemotherapy used in clinical settings, antimitotics (taxanes and/or vinca alkaloids) and anthracycline doxorubicin are two of the most frequently prescribed first-line medications for early breast cancer (Shen and Liu, 2023). Despite their significant efficacy, the evident adverse effects that occur following treatment with these medications make the chemoresistance of breast tumors toward these drugs a major hurdle that can lead to failed treatment (Lovitt et al., 2018; Wanifuchi-Endo

Peer review under responsibility of King Saud University
* Corresponding authors at: Department of Pharmaceutical Chemistry, Faculty of Pharmacy, Universitas Gadjah Mada, Yogyakarta 55281, Indonesia (E. Meiyanto).
E-mail addresses: jkata@bs.naist.jp (J.-y. Kato), edy_meiyanto@ugm.ac.id (E. Meiyanto).
[1] Jun-ya Kato and Edy Meiyanto have equally contributed on the manuscript as corresponding author.

https://doi.org/10.1016/j.jsps.2023.101892
Received 12 May 2023; Accepted 1 December 2023
Available online 2 December 2023
1319-0164/© 2023 The Author(s). Published by Elsevier B.V. on behalf of King Saud University. This is an open access article under the CC BY-NC-ND license (http://creativecommons.org/licenses/by-nc-nd/4.0/).

et al., 2022). As a result, substantial research has been undertaken to identify a rational strategy with several targets for eliminating aggressive breast tumors.

Pentagamavunone-1 (PGV-1) (2,5-bis-(4-hydroxy-3,5-dimethylbenzylidene)-cyclopentanone) is an analog of curcumin that exhibits improved efficacy in eliminating different types of cancer cells compared to curcumin (Meiyanto et al., 2021, 2018). The effects of PGV-1 treatment on cell growth are partly caused by G2/M arrest, which results in senescence and apoptosis (Meiyanto et al., 2019; Novitasari et al., 2023b). PGV-1 inhibits cell migration by decreasing MMP–9 expression, although HER2 expression remains unchanged (Meiyanto et al., 2021; Novitasari et al., 2021a, 2022). PGV-1 was also demonstrated to inhibit tumor growth *in vivo* in a preclinical setting using xenograft models (Kamitani et al., 2022).

Recent studies have indicated that PGV-1 causes prometaphase arrest, as evidenced by the disruption of the nuclear envelope detected via DNA staining (Lestari et al., 2019; Moordiani et al., 2023). During mitosis, the activation of mitotic proteins, such as polo-like kinase 1 (PLK1), Aurora A, and cyclin B1, governs the progression until cytokinesis. These protein kinases are at their peak from mitotic entry to metaphase (Choi et al., 2011; Fu et al., 2007; Schmucker and Sumara, 2014). The most recent work using bioinformatic analysis revealed that PGV-1 may target mitotic proteins (aurora A, cyclin-dependent kinase 1, WEE1, etc.), which probably contributes to its ability to induce mitotic arrest (Meiyanto et al., 2022). While it is well documented that PGV-1 causes prometaphase arrest, the specific molecular mechanism behind this phenomenon is currently unknown. In addition, PGV-1 interacts with NQO2 and GLO1 metabolizing enzymes, resulting in an imbalanced reactive oxygen species (ROS) level that may contribute to cancer cell death (Lestari et al., 2019; Meiyanto et al., 2019). The concern about oxidative stress levels in tumor cells is understandable because tumor cells have higher ROS levels to maintain their metabolism and support uncontrollable proliferation, while the ROS itself can trigger antitumorigenic signaling and initiate oxidative stress-induced tumor cell death (Arfin et al., 2021). Because the majority of ROS production occurs in mitochondria as a result of the oxidative phosphorylation (OXPHOS) process (Dong and Neuzil, 2019; Starkov, 2008), we expect that PGV-1 treatment will also affect mitochondrial function in cancer cells.

This work intends to assess the cellular activities of PGV-1 in breast cancer cells *in vitro* and *in vivo* in order to gain a better understanding of its molecular mechanism in cell cycle progression. Its effects were observed using TNBC and HER2-positive cell lines, which represent aggressive breast cancer cells. This work highlights the effect of PGV-1 on the progression of the cell cycle, which involves the activities of key mitotic kinases (Aurora A, PLK1, and cyclin B1), leading to prometaphase arrest. Furthermore, PGV-1 treatment impairs mitochondrial respiration while enhancing ROS formation due to mitotic arrest. Oral PGV-1 treatment can prevent tumor growth in the cell-derived xenograft model. The present study highlights PGV-1 as a promising chemotherapeutic option for the treatment of breast cancer.

2. Materials and methods

2.1. Compounds and cell lines

PGV-1 was obtained and analyzed at the Cancer Chemoprevention Research Center, Universitas Gadjah Mada (Indonesia). Curcumin (>65%, Sigma-Aldrich, USA, Cat #C1386) and doxorubicin hydrochloride (>90%, Fujifilm Wako Chemical, Japan, Cat #040-21521), as reference chemotherapy for breast cancer cells, were purchased commercially.

The MDA-MB-231 and HCC1954 cell lines were obtained from the American Type Culture Collection (ATCC, USA) and cultured in DMEM and RPMI 1640, respectively. All media contained 10% fetal bovine serum (Hyclone, USA) and 1% penicillin/streptomycin (Fujifilm Wako Chemical, Japan). Adult dermal fibroblasts (NHDF) were purchased from Promo Cell, Germany (Cat #C-12302) and were cultured in fibroblast growth medium (Cat #C-23020) according to the manufacturer's instructions. All cells were stored in a 37 °C, 5% CO_2, humidified incubator.

2.2. Growth curve analysis

A total of 2×10^4 cells were plated into 48-well plates and subsequently exposed to various concentrations of PGV-1. Following a 96 h incubation period, cells were collected using trypsin–EDTA, and then stained with 0.4% trypan blue (Fujifilm Wako Chemical, Japan, Cat #204-21102) so the viable cells could be counted. The percentage of living cells and the growth inhibitory effect at the 50% (GI_{50}) value were determined for each cell line.

To determine the selectivity index (SI) score, the GI_{50} value in NHDF cells was divided by the GI_{50} value of the cancer cells (Indrayanto et al., 2021; López-Lázaro, 2015). According to Weerapreeyakul et al. (2012) and Bézivin et al. (2003), an SI value larger than 3 categorizes a substance as a potential anticancer drug.

The cells were exposed to PGV-1 for 72 h before being drug-washed and replaced with new medium (without PGV-1). For the subsequent 48 h, the cells were kept in incubators. Trypan blue exclusion was performed daily to determine the number of living and dead cells (Lestari et al., 2019).

2.3. Cell cycle analysis

The cells were incubated with PGV-1 for durations of 24, 48, and 72 h. Propidium iodide (PI) solution (Sigma-Aldrich, USA) was used to stain the cells after they were harvested at the end of the treatment. Cells were filtered and collected in a tube, and then analyzed using a FACSCalibur (BD Biosciences) flow cytometer to determine the cell cycle phase distribution (Larasati et al., 2018).

2.4. Double staining with annexin v and PI

After 72 h treatment with PGV-1, cells were harvested by trypsinization and collected for the annexin V/PI binding assay. Cells were resuspended in 100 μL of binding buffer, double-labeled with FITC-annexin V and PI (BD Pharmingen, USA, Cat #556547), and incubated for 10 min. Immediately after the addition of 200 μL of 1 × binding buffer, cells were analyzed using a FACSCalibur flow cytometer (BD Biosciences) (Novitasari et al., 2021b).

2.5. Mitotic index determination

Following 24 h of treatment with 2 μM PGV-1, the cells were collected and incubated for 6 min in 5.6% KCl. Upon centrifugation, the cells were preserved in a 1:3 v/v combination of acetic acid and methanol and carefully dropped on sterile microscope slides. Hoechst 33324 (Cell Signaling Technology, USA, Cat #4082) was added to the slides, and the slides were incubated for 1 h prior to observation under a confocal microscope (Leica Zeiss LSM710) (Lestari et al., 2019). The mitotic index was determined by dividing the number of cells that had undergone mitosis by the total number of cells.

Separately, the cells on the slide were treated for 5 min with May-Grünwald (Sigma-Aldrich, Germany, Cat #63590). The slide was rinsed briefly in phosphate buffer before being immersed in Giemsa's azur solution (Sigma-Aldrich, Germany, #1.09204.0103) for 20 min. The slide was then cleaned with phosphate buffer for 1.5 min. Following a quick rinse in deionized water, the slides were examined under phase-contrast microscopy (Lestari et al., 2019).

2.6. Immunoblotting

Whole-cell lysates were prepared from the cells treated with 2 μM PGV-1 (24 h) by collecting them in a lysis buffer for protein extraction. The lysates were denatured before being loaded onto 10% SDS-PAGE gel, then blotted onto a PVDF membrane. The blots were blocked with 5% BSA prior to incubation with the target antibodies. All the phosphorylated antibodies, including phospho-cyclin B1 (Cat #4133), phospho-PLK1 (Cat #9062), and phospho-Aurora A kinase (Cat #3079), were obtained from Cell Signaling Technology (USA); as well as total protein of Aurora A kinase (Cat #12100) and β-actin (Cat #3700). PLK-1 antibody was purchased from Abcam (USA, Cat #ab17056) and cyclin B1 was obtained from Santa Cruz (Cat #sc-752). The antibodies were dissolved in 5% BSA in PBS (with 0.05% sodium azide) (1:1000 v/v), and phosphorylated antibodies were dissolved in Can Get Signal solution (Toyobo, Japan, Cat #NKB-101) (1:500 v/v). After probing with the primary antibody, the membrane was incubated with secondary antibodies (Cytiva, UK) for antimouse (Cat #NA931V) or antiprotein A (Cat #NA9120V). Detection was performed using enhanced chemiluminescence (ECL) (Cytiva, UK, Cat #RPN2106), and the protein bands were exposed using x-ray film (Fujifilm, Japan, Cat #4741026617). The intensity of each protein band was quantified using ImageJ software (NIH, USA). The expression of each target protein was analyzed by comparing it with the expression of β-actin (with normalization expressed as the fold change relative to the untreated group), then the ratio of phosphorylated protein to total protein was calculated.

2.7. Senescence assay

Following 24 h treatment with PGV-1, the cells were fixed in 4% formaldehyde for 10 min and washed with 1 × PBS. Then, 0.2% X-gal solution was added to the cells, and the cells were incubated before being observed under phase-contrast microscopy (Debacq-Chainiaux et al., 2009).

2.8. Intracellular ROS level measurement

Prior to the treatment, the cell suspension was added to 270 μL of supplemented buffer (containing 10% FBS in 1 × PBS) and stained with 30 μL of 2′,7′-dichlorofluorescin diacetate (DCFDA) solution (final concentration: 20 μM) (Sigma-Aldrich, USA, Cat #D6883). The cells were stored in an incubator for 30 min, then PGV-1 was added to the microtube. The microtube was placed back in the incubator, which was set for three interval times (4, 8, and 24 h). The ROS intensity was determined using flow cytometry, then the mean fluorescence was normalized against the untreated group (Sarmoko et al., 2023).

2.9. Mitochondria respiration analysis

Cells were treated with PGV-1 for 24 h in a 35-mm culture dish. Following trypsinization, MDA–MB-231 (2.25×10^5 cells) and HCC1954 (1.5×10^5 cells) cells were dissolved in assay medium containing 10 mM glucose, 2 mM glutamine, and 1 mM pyruvate and equally distributed in a Cell-Tak (Corning, USA, Cat # 354240) precoated miniplate. After spinning down the 8–well plate for cell adhesion, it was incubated for 30 min. Mito test kit reagents (Agilent, Germany, Cat #103010–100) containing FCCP (1 μM), oligomycin (1.5 μM), and rotenone/antimycin (0.5 μM) were injected into the cartridge, then the oxygen consumption rate (OCR) was recorded using an Agilent XF HS mini analyzer. Finally, the cells were measured for total protein to normalize the OCR data and later analyzed using the Seahorse Analytics platform (https://seahorseanalytics.agilent.com/#) (Novitasari et al., 2023a; Reda et al., 2019).

2.10. Xenograft assay

Female nude mice (*nu/nu*) were used for this experiment. Nude mice are characterized as hairless mice with a lack of thymus; therefore, they have defects in immune function due to T cell deficiency (McDermott-Lancaster et al., 1987). Due to their high vulnerability to bacterial and viral pathogens, the mice were kept in specific-pathogen-free animal house. The animal house had an equal light–dark cycle, a constant temperature ranging from 23 °C to 24 °C, and 50–70% humidity. Mice had free access to autoclaved water and sterile food. The NAIST Institutional Animal Care and Use Committee approved the protocol for the relevant aspects of the animal-related experimental tests (reference number: 1805).

Subcutaneous injections of 1×10^7 cells (in 0.1 mL of culture medium) were made into the flanks of the mice on day 0. Simultaneously, the mice were treated orally with 25 mg/kg BW PGV–1, as reported in the study by Kamitani et al. (2022). PGV-1 was administered orally every 2 days, and the tumor size was recorded during that time. The tumor was excised at the completion of the experiment and weighed using an analytical balance.

2.11. Statistical analysis

Statistical analysis was conducted using the unpaired T-test. A p value of < 0.05 was considered statistically significant, and the graphs were created in GraphPad (version 9.0). Results were reported as the mean ± standard deviation (SD). All p-values were inserted in each figure.

3. Results

3.1. PGV-1 exhibits cytotoxic and antiproliferative effects on breast cancer cells

The antiproliferative properties of PGV-1 were assessed in MDA-MB-231 (triple-negative) (Fig. 1A), HCC1954 (HER2-positive) (Fig. 1B), and NHDF (fibroblast) cells (Fig. 1C). Following a 96 h incubation with PGV-1 (dosage range of 0.001–10 μM), PGV-1 exhibited a substantial cytotoxic effect, with a GI_{50} score of 0.9 ± 0.46 μM for MDA-MB-231 cells, 0.4 ± 0.12 μM for HCC1954 cells, and 3.5 ± 1.08 μM for NHDF cells (Fig. 1D). The similar GI_{50} values in the MDA–MB–231 and HCC1954 cells indicated that breast cancer cells are sensitive to PGV-1.

We also tested the same cell lines with curcumin and the chemotherapy drug doxorubicin (a common option for breast cancer therapy). While doxorubicin was found to be the strongest agent to eliminate these cancer cells, the antiproliferative profile of PGV-1 demonstrated similarity to that of curcumin in HCC1954 cells. However, in MDA-MB-231 cells, PGV-1 was revealed to be three times more potent than curcumin. PGV-1 also demonstrated low antiproliferative activity when tested in normal fibroblast cells, demonstrating its selectivity for cancer cells, with a SI value greater than 3 (Fig. 1D). Based on these results, we attempted to observe the cellular and molecular activities of PGV-1 in MDA-MB-231 and HCC1954 cells.

PGV-1 suppressed MDA-MB-231 cell growth ($p < 0.0001$) and induced cell death ($p < 0.05$) after 96 h of treatment (Fig. 2A). PGV-1 also had an antiproliferative effect in HCC1954 cells, as evidenced by a significant reduction in viable cells ($p < 0.001$), followed by an increasing percentage of dead cells ($p < 0.05$) up to the 4th day (Fig. 2B). Owing to the high chance of treatment failure in breast cancer therapy due to relapse, PGV-1 was cultured in cell medium for 72 h before being replaced without the compound. A lack of expansion in viable MDA-MB-231 cells with a steadily rising percentage of dead cells ($p < 0.01$) suggested that PGV-1 irreversibly inhibited cell growth (Fig. 2C). Even after removal of PGV-1 from the medium, cell growth suppression was still evident, and HCC1954 cells gradually lost their viability ($p < 0.01$) (Fig. 2D). Therefore, PGV-1 demonstrates an irreversible

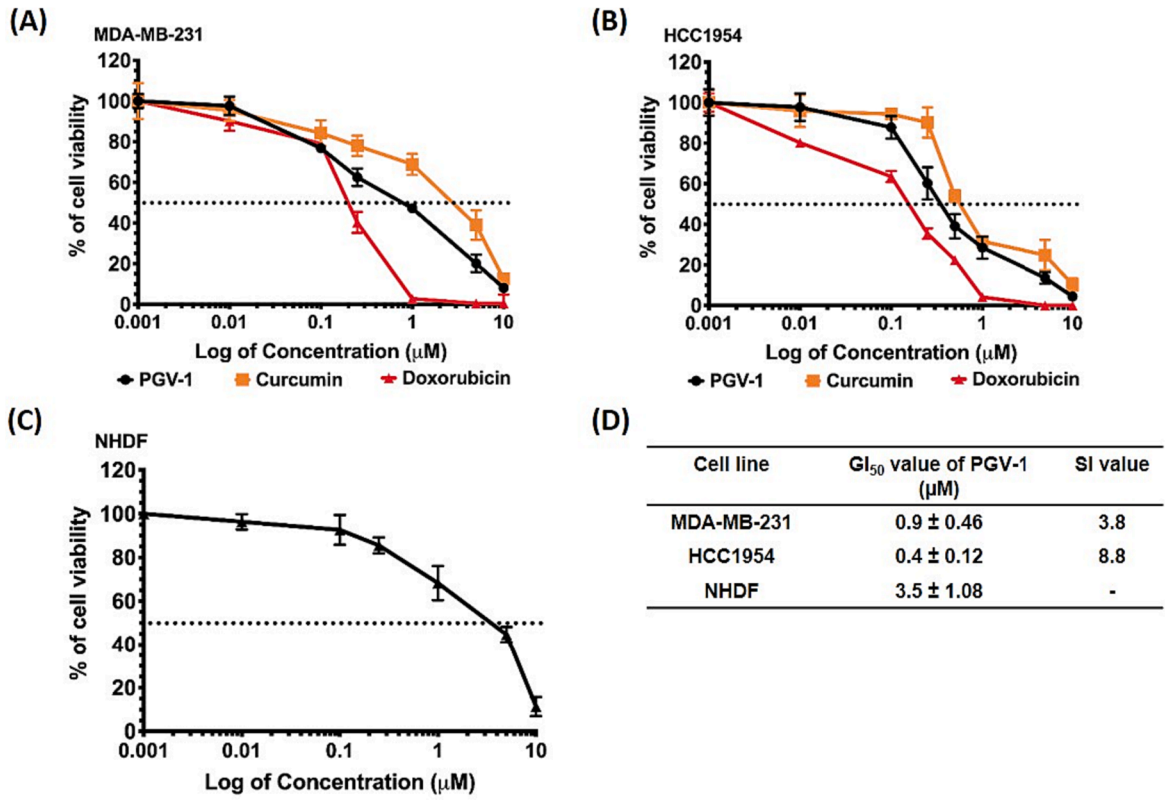

Cell line	GI_{50} value of PGV-1 (μM)	SI value
MDA-MB-231	0.9 ± 0.46	3.8
HCC1954	0.4 ± 0.12	8.8
NHDF	3.5 ± 1.08	-

Fig. 1. PGV-1 inhibits breast cancer cell growth. (A) MDA-MB-231 and (B) HCC1954 cells growth curves upon PGV-1 treatment, along with curcumin and doxorubicin as reference compounds (C) The growth from NHDF cells that were treated with PGV-1 (D) The GI_{50} and selectivity index (SI) values of PGV-1. Results are expressed as mean ± SD of triplicate samples.

antiproliferative effect on breast cancer cells.

3.2. PGV-1 triggers mitotic arrest in breast cancer cells

To achieve a better understanding of how PGV-1 hinders cell growth, we exposed cells to 2 μM PGV-1 for 24, 48, and 72 h and analyzed their cell cycle profiles. PGV-1 halted MDA-MB-231 cells at G2/M within the first 24 h (51.8% ± 9.4% versus 19.6% ± 1.2% of untreated cells, $p < 0.01$) (Fig. 3A and 3B). Exposure to PGV-1 prompted the cells to arrest in G2/M, then gradually shift into hyperploid stage arrest (7.4% ± 3.5% at 24 h versus 14.3% ± 15.0% at 72 h), indicating the failure of cell division. The subG1 cell population was also found to be increased in the PGV–1-treated group at the end of the observation (11.7% ± 6.0% versus 4.9% ± 4.1% in the untreated group at 72 h). In HCC1954 cells, PGV-1 caused G2/M arrest (37.8% ± 7.8% versus 23.9 ± 3.6% in the untreated group, $p < 0.05$) after the first 24 h of treatment. However, the effect of PGV-1 was diminished during longer exposure times (18.4% ± 5.0% at 48 h and 13.7% ± 4.4% at 72 h) (Fig. 3C and 3D). In contrast to MDA-MB-231 cells, hyperploid HCC1954 cells were absent following PGV-1 treatment. This phenomenon was followed by cell accumulation at subG1 in PGV-1-treated HCC1954 cells, starting at 15.1% ± 12.1% at 24 h and reaching 41.8% ± 24.2% after 72 h, which was 2.7 times higher than the untreated group (15.3% ± 4.3% at 72 h). These data imply that PGV-1 inhibits cell growth mainly during G2/M phase.

Since 72 h posttreatment showed the cell population in subG1, we determined the apoptosis incidence through double labeling with annexin V (AnxV) bound to phosphatidylserine (PS) from the inner cell membrane and PI to stain the DNA. The flow cytogram showed that, after PGV-1 exposure, some MDA-MB-231 (Fig. 4A) and HCC1954 (Fig. 4B) cells were labeled with both AnxV and PI. The quantification results showed that there was a drastic increase ($p < 0.0001$) in $AnxV^+/PI^+$- and $AnxV^+/PI^-$-labeled cells after PGV-1 treatment in MDA-MB-231 cells, suggesting that PGV-1 may trigger apoptosis. We also noticed an increasing percentage in the double-positive (Anx^+/PI^+) population ($p < 0.0001$) after PGV-1 exposure in HCC1954 cells. However, Anx^-/PI^+ cells were also detected in the HCC1954 cells (Fig. 4D), indicating damage to the cell membrane, enabling PI to bind with DNA. These results support the notion that PGV-1 has the potential to induce apoptosis in breast cancer cells.

Because PGV-1 induced G2/M arrest, a follow-up experiment was conducted using chromosomal staining to determine whether PGV-1 halted the cell cycle at the Gap2 (G2) phase or the mitosis phase. The observations from the Giemsa staining demonstrated that PGV-1 caused aberrant chromosomal condensation and disappearance of the nuclear envelope membrane, indicating that many cells were arrested at mitosis (Fig. 5A). The quantification analysis revealed that PGV-1 dramatically ($p < 0.01$) increased the percentage of mitotic cells from 3.7% ± 2.7% to 15.1% ± 2.1%. Similarly, PGV-1 increased ($p < 0.05$) the number of mitotic HCC1954 cells.

The chromosome was also stained with Hoechst and then viewed under confocal microscopy to establish the precise mitotic stage after PGV-1 treatment. PGV-1 caused prometaphase arrest in the mitotic phase, as indicated by chromosomal condensation and segregation upon nuclear envelope breakdown, meaning the cells could not properly move to the equatorial plane (Fig. 5B). The results of the mitotic index calculation showed that PGV-1 significantly ($p < 0.05$) induced mitotic cell formation (17.5 ± 3.5) compared to the untreated group (0.3 ± 0.5) in MDA-MB-231 cells. A similar finding was observed in HCC1954 cells, as prometaphase-arrest cells were present in the PGV-1 group, with a mitotic index of 2.8 ± 0.6, which was higher than that of the untreated group (0.2 ± 0.3). These results suggest that PGV-1 targets the cell cycle progression of breast cancer cells during prometaphase.

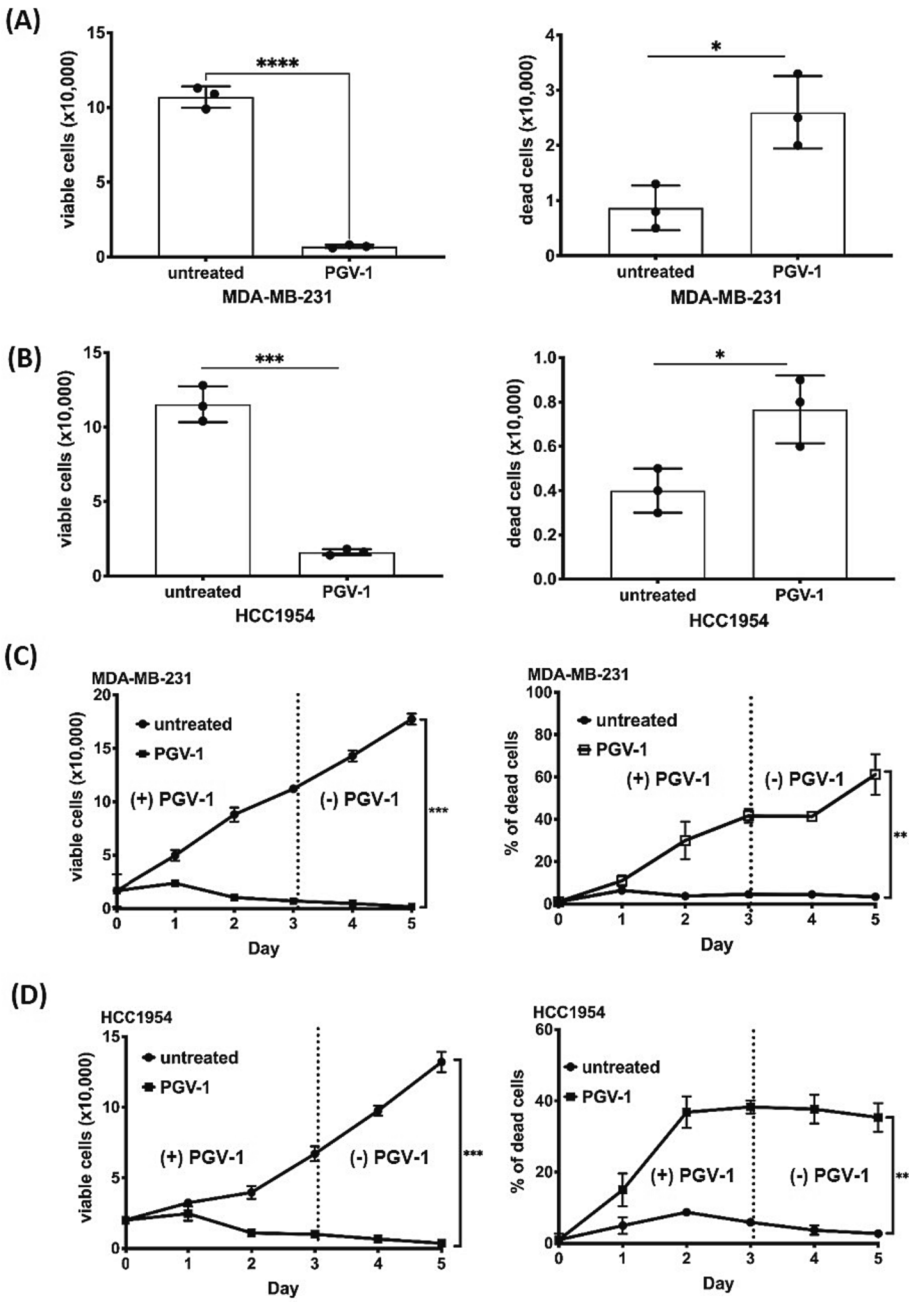

Fig. 2. PGV-1 inhibits breast cancer cell growth in an irreversible manner. (A) The viable cells and dead MDA-MB-231 and (B) HCC1954 cells after 2 μM PGV-1 treatment for 96 h. (C) The growth curve of viable and cell death percentage of MDA-MB-231 and (D) HCC1954 cells after removal of 2 μM PGV-1 from culture medium. Results are displayed as average ± SD ($n = 3$). (*$p < 0.05$; **$p < 0.01$; ***$p < 0.001$; ****$p < 0.0001$).

3.3. PGV-1 causes mitotic arrest through mitotic kinase activation in breast cancer cells

Next, we examined the protein levels of major mitotic regulators, such as Aurora A kinase, PLK1, and cyclin B1, including both the total protein and its phosphorylated form (Fig. 6A). The phosphorylation of Aurora A kinase was not affected in HCC1954-treated cells, in contrast with the result in MDA-MB-231 cells (Fig. 6B). PLK1 phosphorylation was enhanced ($p < 0.05$) in both cell lines (Fig. 6C), indicating PGV-1 activity during mitosis. Meanwhile, cyclin B1 activation upon PGV-1 treatment was increased and notably higher ($p < 0.05$) in HCC1954 cells than in MDA-MB-231 cells (Fig. 6D). Based on these findings, it appears that the mitotic arrest induced by PGV-1 is mediated by a distinct set of related regulators with respect to its activity in breast cancer cells.

3.4. PGV-1 promotes senescence in breast cancer cells

Since PGV-1-treated cells did not perish within 24 h but were halted in mitosis, the mechanism behind this occurrence was investigated further. Therefore, we evaluated whether PGV-1 also triggered senescence (stable proliferation arrest) in aggressive breast cancer cells. PGV-1 treatment significantly ($p < 0.05$) promoted MDA-MB-231 cell senescence by 30.5% ± 12.6% (Fig. 7A). A similar phenomenon was observed in the HCC1954 cells, where PGV-1 exposure enhanced cell senescence by 29.1% ± 4.0% ($p < 0.001$) (Fig. 7B). These findings reveal that PGV-1-induced senescence may be associated with decreased cell viability and extended cell cycle arrest.

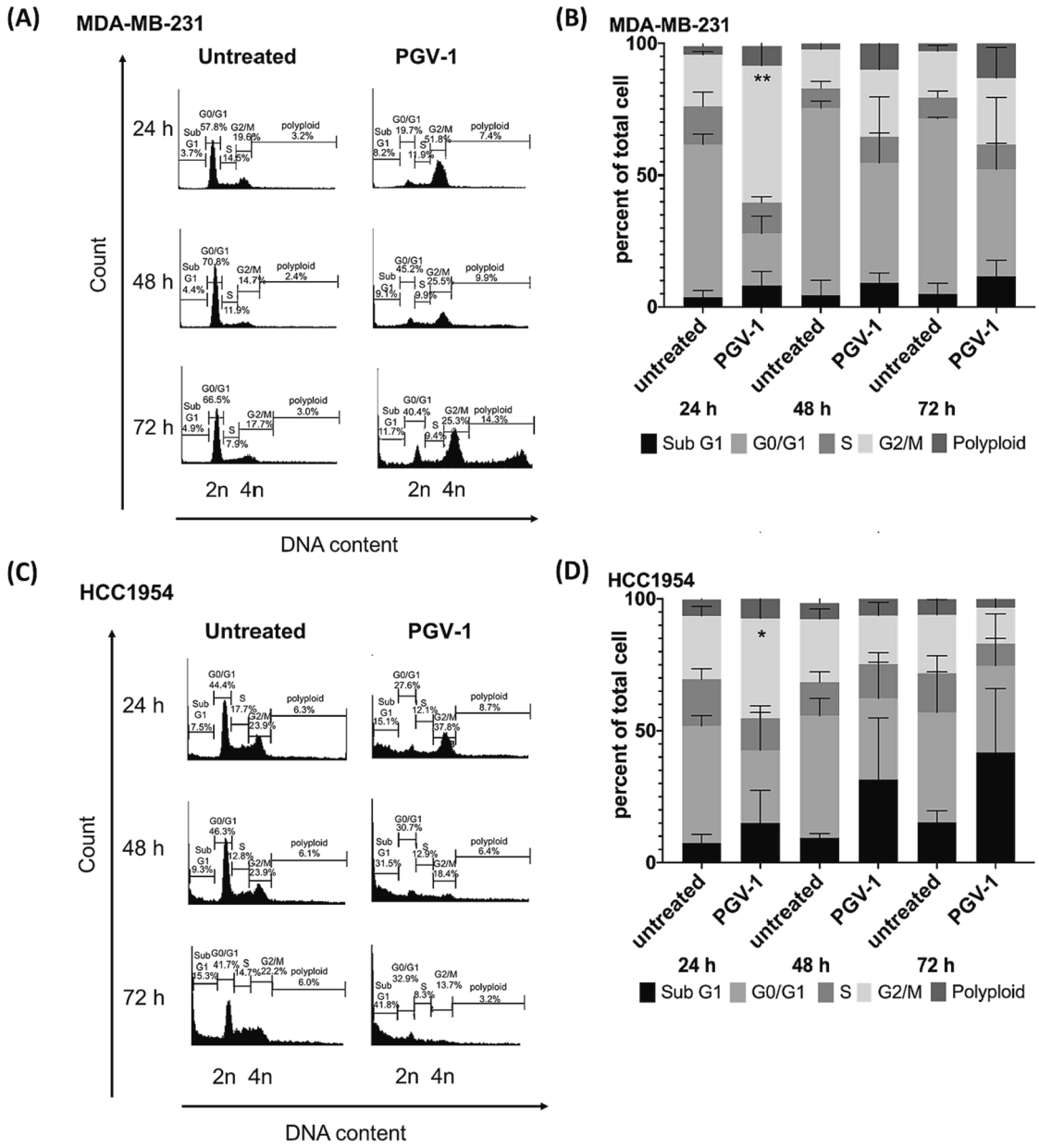

Fig. 3. PGV-1 induces G2/M arrest during cell cycle progression. (A) Flow cytogram and (B) MDA-MB-231 cells distribution in each phase after treatment with 2 μM PGV-1 (C) The profile of cell cycle after 2 μM PGV-1 treatment in HCC1954 cells was followed by (D) distribution of cell accumulation in every cell cycle. Results are showed as average ± SD ($n = 3$). (*$p < 0.05$ and **$p < 0.01$ compared to untreated).

3.5. PGV-1 enhances ROS production and impairs mitochondrial respiration

Cellular senescence is commonly associated with harmful cellular species, such as ROS (Davalli et al., 2016). Our data showed that PGV-1 induced cellular senescence in breast cancer cells; therefore, we measured the ROS level to understand the correlation between these two phenomena. In MDA-MB-231 cells, PGV-1 exposure caused a significant increase in ROS level ($p < 0.01$) even after only 4 h of incubation, and this elevated ROS level was maintained until 24 h. Similarly, the ROS levels remained noticeably ($p < 0.01$) greater in the PGV-1-treated HCC1954 cells compared to the untreated HCC1954 cells (Fig. 8A). These findings suggest that ROS generation is a potential cellular mechanism of PGV-1 to induce senescence and mitotic arrest.

When ROS levels are elevated, mitochondria are damaged due to changes in their respiratory chain and membrane permeability (Sullivan and Chandel, 2014). The cellular OCR was measured as a marker of mitochondrial respiration to see how PGV-1 treatment affected mitochondrial function (Fig. 8B). After 24 h of treatment, the maximal respiration was suppressed ($p < 0.05$) in HCC1954 cells, but not in MDA-MB-231 cells (Fig. 8C). PGV-1 treatment suppressed the ATP-linked respiration in MDA-MB-231 ($p < 0.001$) but not in HCC1954 cells (Fig. 8D). Also, PGV-1 treatment reduced basal respiration ($p < 0.001$) in MDA-MB-231 cells; however, the level was unaltered in HCC1954 cells (Fig. 8E). These results indicate that PGV-1 triggers mitochondrial dysfunction in breast cancer cells, possibly due to increased production of ROS.

3.6. PGV-1 inhibits tumor formation in xenograft models

The antitumorigenesis effect of PGV-1 was also evaluated *in vivo* using a xenograft model. Athymic-nude mice bearing MDA-MB-231 or

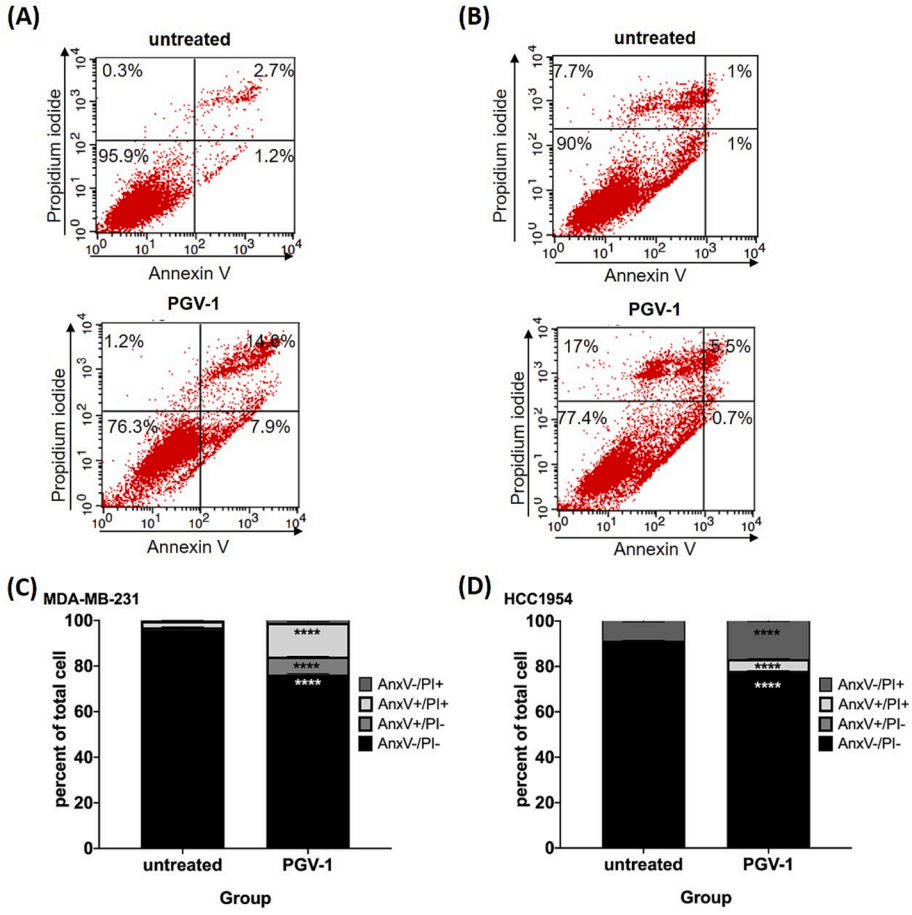

Fig. 4. PGV-1 triggers cell apoptosis. (A) MDA-MB-231 and (B) HCC1954 cells population after exposure of 2 μM PGV-1 for 72 h based on apoptosis quadrant after labeling with Annexin V (AnxV) - propidium iodide (PI). Results are showed as average ± SD ($n = 3$). (****$p < 0.0001$ compared to untreated).

HCC1954 cells were established by subcutaneously injecting cells into the flank, followed by treatment with 25 mg/kg BW PGV-1 every 2 days. PGV-1 suppressed tumor growth ($p < 0.01$) (Fig. 9A), though the weight of the tumor nodules were not significantly repressed in MDA-MB-231-xenograft mice (Fig. 9B and 9C). The study using the HCC1954 xenograft model also showed that the oral administration of 25 mg/kg BW PGV-1 effectively and significantly ($p < 0.01$) repressed the tumor size to 157 mm^3 compared to the untreated group (992 mm^3) (Fig. 9D). The tumor also shrank significantly ($p < 0.001$) after treatment with PGV-1 (95 mg versus 290 mg in the untreated group) (Fig. 9E and 9F). These results confirm that PGV–1 demonstrates a tumor-suppressing effect *in vivo*.

4. Discussion

This study was designed to evaluate the anticancer activity of monocarbonyl PGV-1 against highly aggressive breast cancer cells. Other studies employing different breast cancer cell lines, such as luminal MCF-7 and T47D cells (Meiyanto et al., 2014; Wulandari et al., 2020), HER2-overexpressed MCF7 cells (Meiyanto et al., 2021), and triple-negative 4 T1 cells (Meiyanto et al., 2019), have revealed the anticancer properties of PGV-1. Through this study, we were able to determine that PGV-1 irreversibly inhibits cell proliferation in the two most aggressive breast cancer subtypes (triple-negative MDA-MB-231 and HER2-amplified HCC1954), which may potentially lower the risk of tumor recurrence after treatment. Therapeutic selectivity is one of the most crucial aspects of cancer treatment (Atkins and Gershell, 2002), and we also observed the selectivity of PGV-1 in non-cancerous cells. Our results showed that PGV-1 is selective in inhibiting cancer cell proliferation, as it did not affect fibroblast cells; this is consistent with the results reported for epithelial kidney cells (Meiyanto et al., 2021). These preliminary data promote further investigation of PGV-1 to determine its underlying molecular mechanism in breast cancer cells.

Our results showed that PGV-1 triggers cell cycle arrest in the prometaphase, suggesting that, regardless of cancer cell type, PGV-1 acts similarly in inhibiting mitosis progression (Lestari et al., 2019; Moordiani et al., 2023). Interestingly, PGV-1 promoted hyperploid formation in MDA-MB-231 cells after prolonged incubation, indicating that mitotic failure may occur. Prolonged arrest in mitosis (notably in prometaphase or metaphase) can cause tetraploidization upon trigger from chemotherapy, which prompts the cells to exit mitosis without undergoing cytokinesis (Haschka et al., 2018). Conversely, the polyploid characteristics were absent in HCC1954 cells following PGV-1 treatment. One possible explanation for this finding is that a substantial number of cells had already entered the subG1 phase after 24 h of PGV-1 exposure (<2N), showing that HCC1954 cells are more responsive to PGV-1 than MDA-MB-231 cells. SubG1 populations are frequently associated with the occurrence of apoptosis due to reduced DNA content (Plesca et al., 2008). Since the subG1 phase is generally defined as having fragmented DNA content, we further evaluated this finding via Annexin V-PI double labeling to identify the initial stage of apoptosis. The findings demonstrated that PGV-1 increased the proportion of early and late apoptotic (Annexin V-labeled) cells in MDA-MB-231 cells compared to HCC1954 cells. The presence of permeabilized HCC1954 cells (marked by $AnxV^-/PI^+$) following PGV-1 treatment indicated that the treatment may induce cell membrane perturbation, one of the phenomena observed in cellular cytotoxicity. In this case, the membrane damage caused by PGV-1 caused cells to be positively stained with PI only (as seen in the population of $AnxV^-/PI^+$ cells). Since this technique is time-sensitive, even

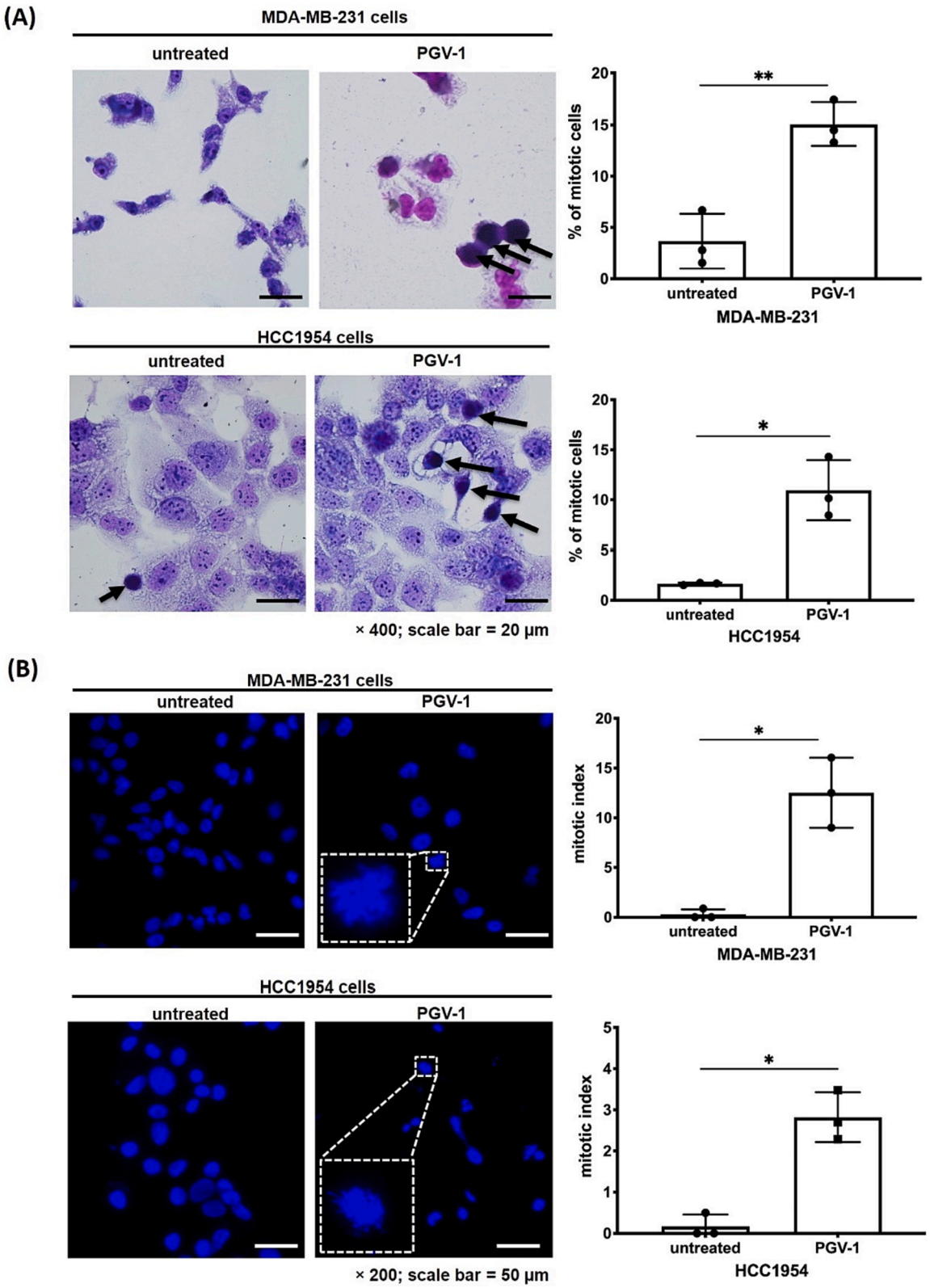

Fig. 5. PGV-1 induces prometaphase arrest during the mitosis. (A) The MDA-MB-231 and HCC1954 cells morphology upon staining with May–-Grünwald–Giemsa (MGG), following by the calculation of %mitotic cells after 24 h incubation with 2 µM PGV-1. The appearance of mitotic cells is indicated by the black arrow (B) The DNA-bind Hoechst 33342 labeling in treated cells, followed by quantification for mitotic index. The enlarged cells image displayed the prometaphase-arrest cell. The results are reported as average ± SD ($n = 3$) (*$p < 0.05$ and**$p < 0.01$).

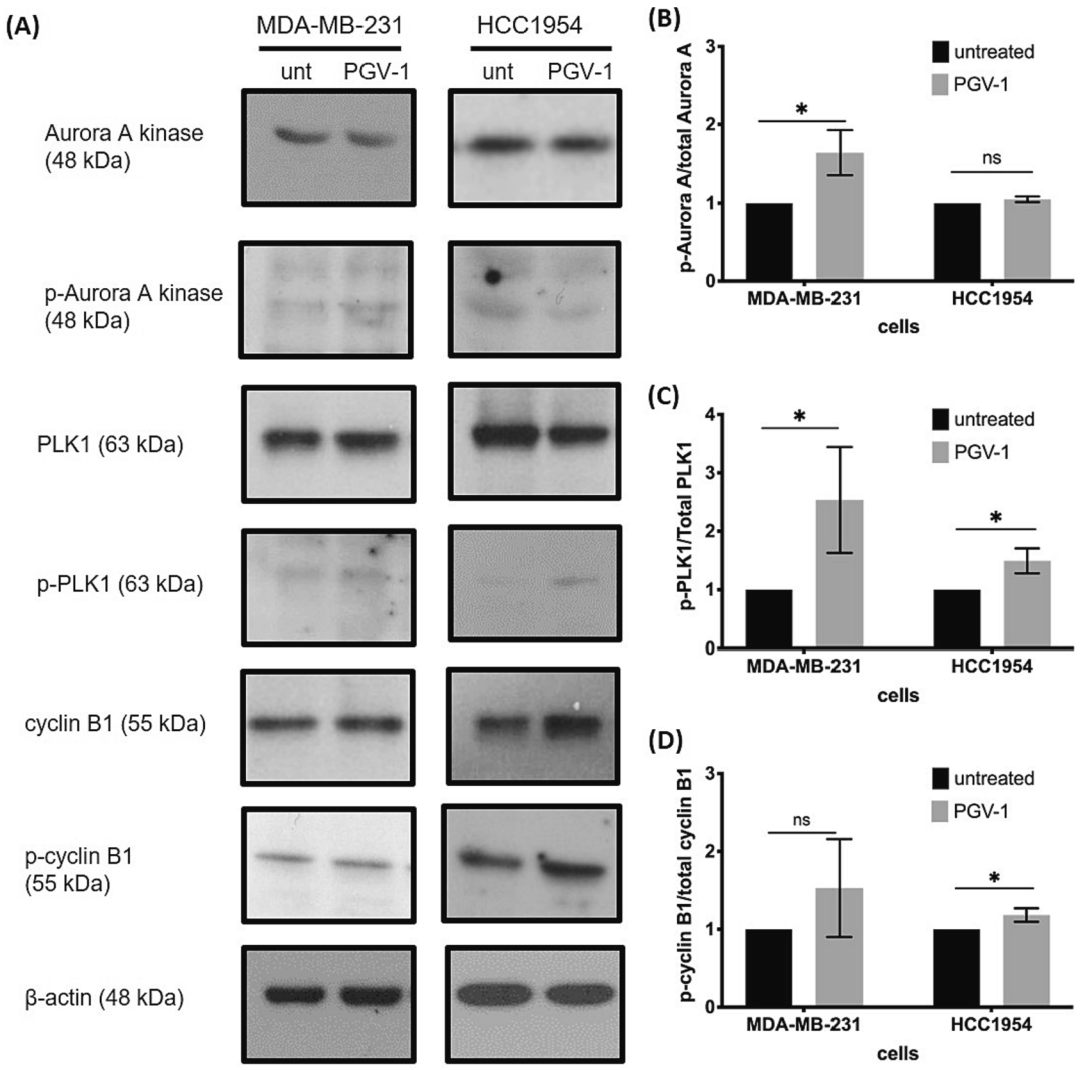

Fig. 6. PGV-1 phosphorylates mitotic kinases. (A) Immunoblot presentation of PGV-1-treated lysates in MDA-MB-231 and HCC1954 cells, later followed by quantification for the intensity of (B) phospho-Aurora A, (C) phospho-PLK1, and (D) phospho-cyclin B1 against its total protein. The histogram is displayed as average ± SD ($n = 3$) (ns: not significant; $^*p < 0.05$).

live cells can be permeable to PI during a prolonged incubation period. Furthermore, at an early phase of apoptosis, partial DNA content (subG1 fraction) can be positive in exposed PS residue (Darzynkiewicz et al., 2001), which also explains why the proportion of the subG1 population was different from the distribution in the apoptosis assay. PGV-1 is known to induce PUMA and BAX expression and to trigger PARP cleavage in MCF-7 cells (Da'i et al., 2017). Therefore, a different approach should be employed to assess the apoptosis incidence after PGV-1 treatment.

In another context, subG1 populations can also arise from the accumulation of uneven DNA content (i.e., from hypodiploid and hyperdiploid cells) due to transient mitotic arrest caused by antimitotic drugs (Demidenko et al., 2008). Certain mitotic cells emerge in subG1 due to micronuclei or DNA fragmentation caused by mitotic catastrophe (Kawamura and Fujikawa-Yamamoto, 2009). This may also occur in response to PGV-1 treatment to induce mitotic catastrophe before entering the apoptosis stage.

Since this study confirms the activity of PGV-1 in inhibiting mitotic progression in breast cancer cells, we observed whether the mitotic kinases were also altered by this compound. Our results showed that the phosphorylation of Aurora A protein was induced by PGV-1 in MDA–MB–231 cells. During prometaphase, Aurora A participates in the development of centrosomes and the establishment of a bipolar spindle via γ-tubulin signaling (Cowley et al., 2009; Tillery et al., 2018). Aurora A also facilitates γ-tubulin recruitment in prometaphase, even at low protein levels, due to its capability to remain active through autophosphorylation in Thr288. However, this event can lead to centrosome dysfunction after centriole separation breaks down (Marumoto et al., 2003). We also observed PLK1 phosphorylation in PGV-1-treated cells, confirming its peak activity in mitosis. In centrosome maturation during prometaphase, PLK1 acts as part of the Aurora A/CEP192 axis, whereas CEP192 acts as a scaffold for Aurora A and PLK1 and increases their proximity to each other (Asteriti et al., 2015; Joukov and Nicolo, 2018; Park et al., 2023). Consequently, the activity of PGV-1 in prometaphase arrest may involve centrosome activity. Instead of being degraded, PGV-1 also induces the phosphorylation of cyclin B1 in breast cancer cells. During prometaphase, cyclin B1 is located in the centromere and is concentrated in the kinetochore's outer plate along with CDK1 (Yu and Yao, 2008). To guarantee chromosomal adherence to the mitotic spindle, cells must maintain a mitotic state with persistently strong cyclin B1-CDK1 activity (Lindqvist et al., 2007). Cells that are incapable of completing mitosis have unusual morphological nuclear alterations, which are characterized by an aberrant rise in the level of cyclin B1 and a delay in mitotic transition (Castedo et al., 2004). A study with antimitotic nocodazole showed that binding with MAD2 (a mitotic checkpoint complex protein), which accompanied cyclin B1 upregulation,

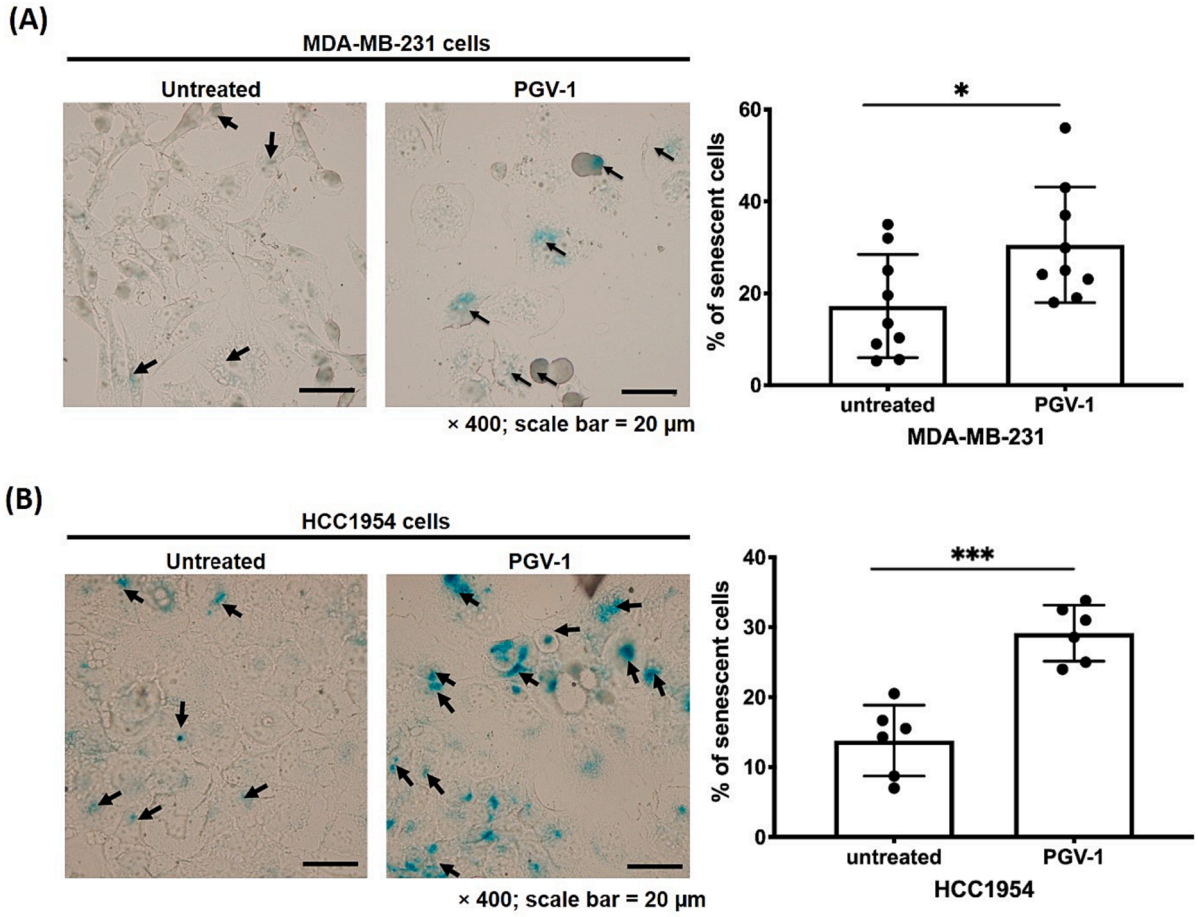

Fig. 7. PGV-1 promotes cellular senescence. (A) The cellular senescence observation and percentage of senescence in MDA-MB-231 ($n = 9$) and (B) HCC1954 cells ($n = 6$) following treatment with 2 µM PGV-1 (24 h). The green-stained cells indicate senescent cells. Results are demonstrated as average ± SD (*$p < 0.05$ and ***$p < 0.001$). (For interpretation of the references to colour in this figure legend, the reader is referred to the web version of this article.)

caused prometaphase arrest in MCF7 cells (Choi et al., 2011). The cyclin B1 upregulation that was related with G2/M arrest was also observed in another report that used TNBC MDA-MB-468 cells treated with sesquiterpene lactones derivates (Chimplee et al., 2022). These cascades suggest that PGV-1 uniquely targets centromere activity during prometaphase, leading to mitotic arrest.

Mitochondrial dysfunction and the subsequent production of elevated ROS impose an immense burden on cancer cells that are halted in mitosis (Kumari et al., 2018; Sullivan and Chandel, 2014). Our findings revealed that in addition to PGV-1-treated cells being primarily arrested at M phase, this curcumin analog generates an increase in ROS formation. Furthermore, the effect of PGV-1 to enhance ROS formation is comparable to that of peroxide, which also escalates the ROS level (Supplementary Fig. 1A–1B) following G2/M arrest (Supplementary Fig. 1C–1D). Prior studies have shown that PGV-1 interacts with ROS-metabolizing enzymes (NQO1, NQO2, and GLO1), which probably mediates the increased ROS level in cancer cells (Lestari et al., 2019; Meiyanto et al., 2021). Wu et al. (2017) discovered that peroxide-induced stress delays prometaphase/metaphase due to spindle assembly checkpoint activation, which is presumably also demonstrated by PGV-1 to enhance prometaphase arrest. The oxidative stress caused by antimitotic chemotherapeutics can have two effects: producing mitotic arrest (Wang et al., 2017) or overriding the mitotic spindle checkpoint, resulting in premature mitotic exit with aneuploidy (D'Angiolella et al., 2007). These findings corroborate the notion that PGV–1-induced oxidative stress is linked to mitotic arrest.

Furthermore, PGV-1 treatment impairs mitochondrial respiration, resulting in ROS accumulation and causing prometaphase arrest. This overburdens mitotic cells with mitochondria that have deteriorated functionally. Mitochondria are crucial for maintaining the intrinsic oxidative stress within tumor cells in order to sustain high cellular metabolism, making them susceptible to greater oxidative stress from exogenous ROS-generating substances (Starkov, 2008). Moreover, mitochondria also fulfill a crucial function in the process of apoptosis by facilitating the release of cytochrome *c* due to alterations in the permeability of the mitochondrial membrane (Chen and Lesnefsky, 2006). Since PGV-1 increases oxidative stress by binding to ROS-eliminating enzymes (Lestari et al., 2019), this finding suggests a potential association between PGV-1 and mitochondrial damage, which leads to an increase in ROS production, inhibition of mitochondrial respiration, and initiation of apoptosis.

The significant increase in galactosidase activity following PGV-1 treatment is evidence that these events can cause cancer cells to experience stress-induced senescence in response to ROS exposure (Barra et al., 2022). In another context, microtubule inhibitors (vinca alkaloids, paclitaxel, and docetaxel) that hinder mitotic arrest by targeting spindle dynamics may also mediate significant DNA damage and initiate senescence (Bojko et al., 2019; Schwarze et al., 2005). It is important to remember that apoptosis typically occurs at greater concentrations of chemotherapeutic drugs, while the senescent cell state is initiated at lower doses (Roninson, 2003). Although some chemotherapeutics can cause senescence, the apoptotic response is prevalent in most tumors (Kaufmann and Earnshaw, 2000). Through this study, we observed that PGV-1 can restrain the cells during mitosis, induce senescence through a catastrophic event, then cause cell death.

The growth of MDA-MB-231 and HCC1954 tumors in xenograft mice

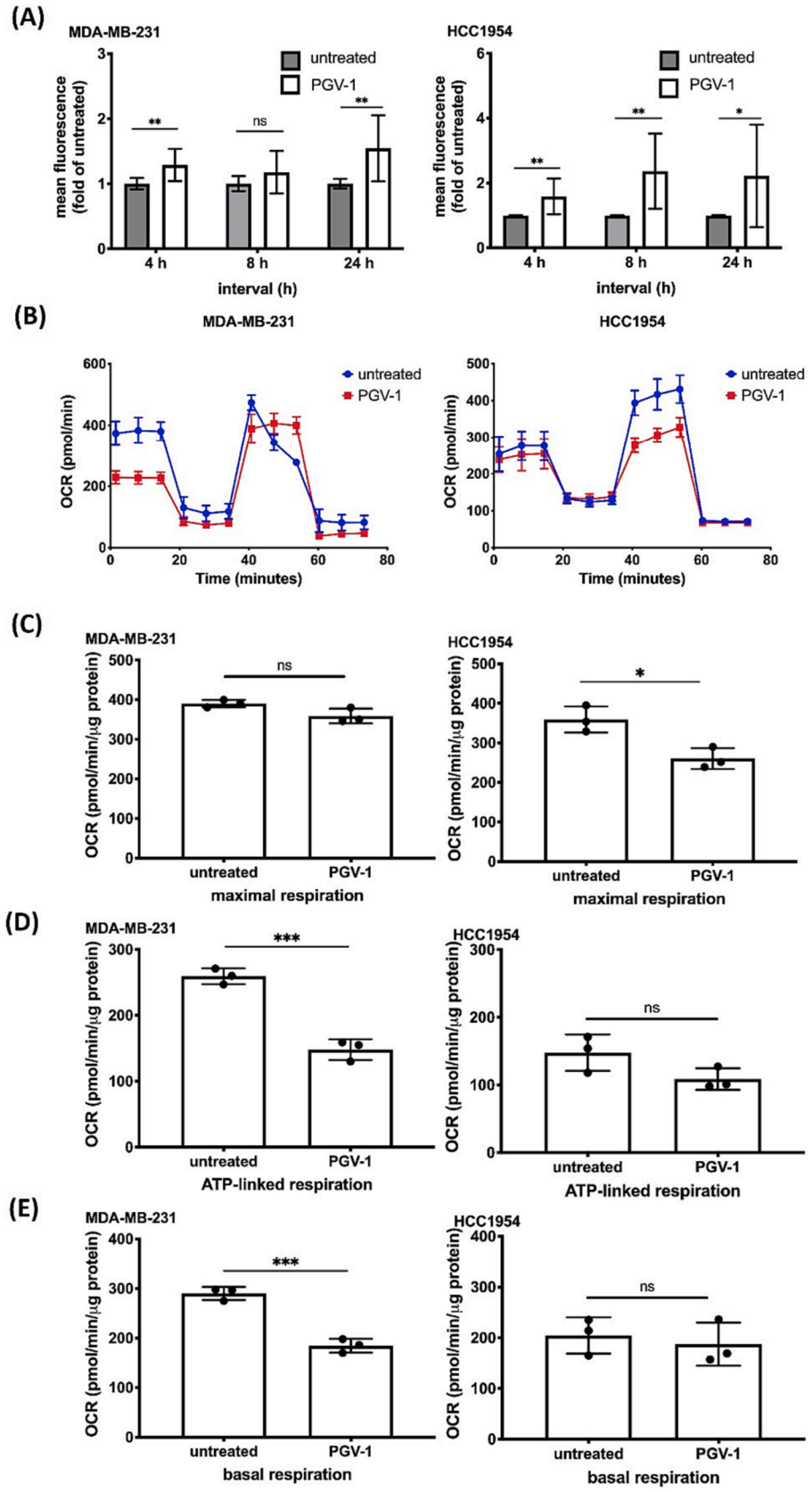

Fig. 8. PGV-1 increases the amount of ROS within the cell and impedes mitochondrial respiration. (A) The cellular ROS intensity following 2 μM PGV-1 treatment in MDA-MB-231 ($n = 9$) and HCC1954 cells ($n = 9$) (B) The graphical representation of oxygen consumption rate (OCR) is analyzed through the Seahorse analytics webtool. The OCR level graph is plotted alongside parameters for (C) maximal respiration, (D) ATP-linked respiration, and (E) basal respiration ($n = 3$). Results are illustrated as average ± SD (ns: not significant; $^{*}p < 0.05$; $^{**}p < 0.01$; $^{***}p < 0.001$).

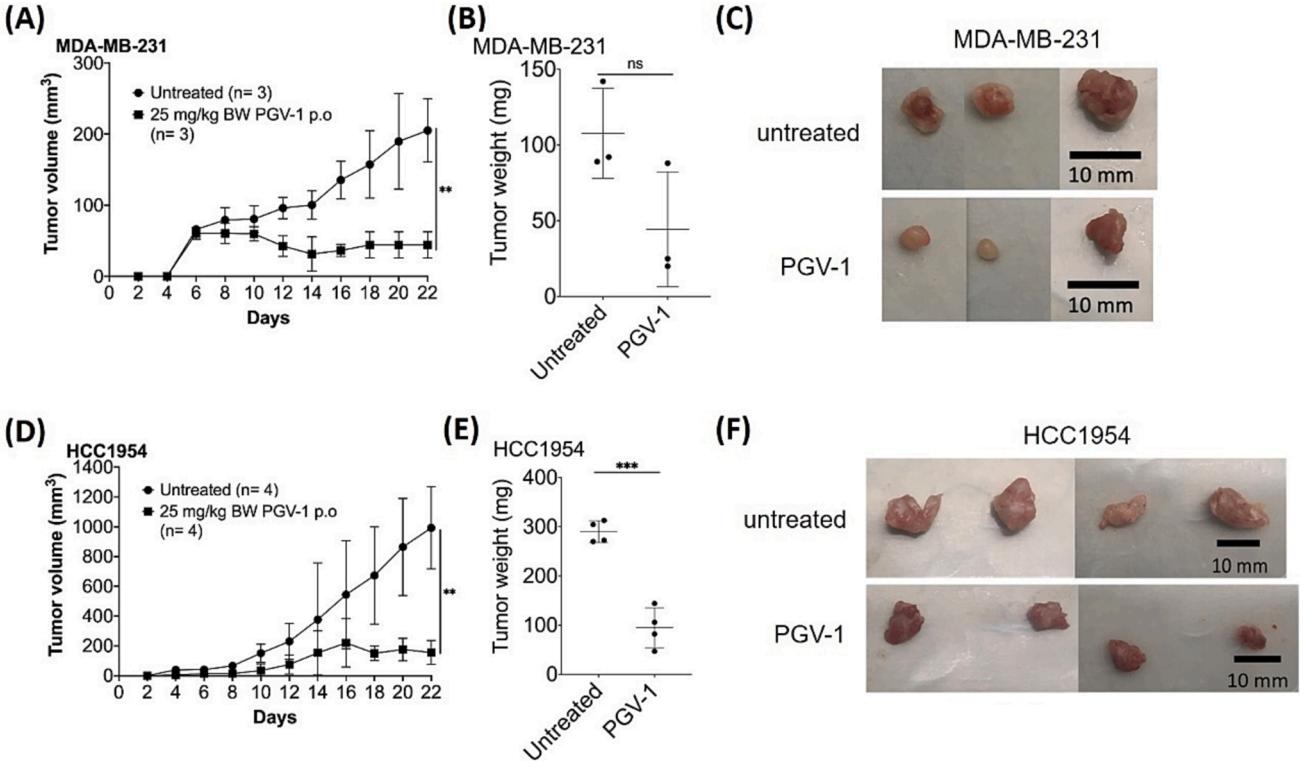

Fig. 9. PGV-1 suppresses the formation of MDA-MB-231 and HCC1954 cell-derived xenograft mice. (A) Tumor volume and (B) Tumor weight from the sacrifice of the mice bearing MDA-MB-231 tumor (C) Graph of tumor volume from HCC1954-xenograft mice (D) was plotted, along with the tumor weight (E) and the appearance of the tumor (F) after the completion of PGV-1 treatment. Data are presented as mean ± SD (***$p < 0.001$; **$p < 0.01$; ns = not significant).

were effectively suppressed by the oral treatment of PGV-1, suggesting that PGV-1 possesses antitumorigenic effects *in vivo*. We realize that these subcutaneous tumors can be altered by variables such as the injection technique, cell line, and growth rate (Brough et al., 2023; Guerin et al., 2020), which may affect tumor size variation. Prior studies in leukemia K562-implanted mice (Lestari et al., 2019) and murine TNBC 4T1-xenograft mice (Meiyanto et al., 2021) also reported similar antitumor evidence for PGV-1. Moreover, PGV-1 treatment in pancreatic cell-derived and patient-derived xenografts have been shown to have no discernible impact on body weight, hematological profiles, or mouse behavior (Kamitani et al., 2022). No abnormalities in rat livers were reported based on the morphology and the expression of Ki-67 following oral administration of PGV-1 for 16 weeks (Novitasari et al., 2023b). Furthermore, the evaluation of acute toxicity following PGV-1 treatment revealed no instances of mortality or significant adverse effects (Tim Molnas Fak. Farmasi UGM, 2001). The results of this study offer more evidence to strengthen the effectiveness of PGV-1 therapy through oral administration, regardless of the specific cancer type or its malignant characteristics. Further experiments using a larger sample size are needed to fully comprehend how PGV-1 exerts its antitumorigenic effects *in vivo*.

5. Conclusion

The findings of this study suggest that PGV-1 disrupts prometaphase, activates mitotic kinases (aurora A, PLK1, and cyclin B1), increases ROS levels, promotes senescence, and impairs mitochondrial respiration to facilitate cell death. Because of its anticancer capabilities, PGV-1 has the potential to become a notable antineoplastic option for malignant breast cancer chemotherapy.

Ethics approval

The NAIST Institutional Animal Care and Use Committee (Japan) permits the use of *in vivo* experimental protocols for this study under the reference number 1805.

Funding

This work is financially supported through Master Education Leading to Doctoral Program for Excellent Graduate (PMDSU) (No. 2328/UN1/DITLIT/DIT-LIT/PT/2021) and "Penelitian Dasar Kemitraan" (No. 2119/UN1/DITLIT/Dit-Lit/PT.01.03/2023) Research Scheme from Ministry of Education, Culture, Research, and Technology, Republic of Indonesia.

CRediT authorship contribution statement

Dhania Novitasari: Methodology, Supervision, Resources, Writing – review & editing. **Ikuko Nakamae:** Methodology, Supervision, Resources, Writing – review & editing. **Riris Istighfari Jenie:** Methodology, Supervision, Resources, Writing – review & editing. **Noriko Yoneda-Kato:** Methodology, Supervision, Resources, Writing – review & editing. **Jun-ya Kato:** Methodology, Supervision, Resources, Writing – review & editing. **Edy Meiyanto:** Methodology, Supervision, Resources, Writing – review & editing.

Declaration of Competing Interest

The authors declare that they have no known competing financial interests or personal relationships that could have appeared to influence the work reported in this paper.

Appendix A. Supplementary data

Supplementary data to this article can be found online at https://doi.org/10.1016/j.jsps.2023.101892.

References

Arfin, S., Jha, N.K., Jha, S.K., Kesari, K.K., Ruokolainen, J., Roychoudhury, S., Rathi, B., Kumar, D., 2021. Oxidative Stress in Cancer Cell Metabolism. Antioxidants. (Basel) 10, 642. https://doi.org/10.3390/antiox10050642.

Asteriti, I.A., De Mattia, F., Guarguaglini, G., 2015. Cross-Talk between AURKA and Plk1 in Mitotic Entry and Spindle Assembly. Front. Oncol. 5 https://doi.org/10.3389/fonc.2015.00283.

Atkins, J.H., Gershell, L.J., 2002. Selective anticancer drugs. Nature. Reviews. Drug. Discovery 1, 491–492. https://doi.org/10.1038/nrd842.

Barra, V., Chiavetta, R.F., Titoli, S., Provenzano, I.M., Carollo, P.S., Di Leonardo, A., 2022. Specific irreversible cell-cycle arrest and depletion of cancer cells obtained by combining curcumin and the flavonoids Quercetin and Fisetin. Genes. (Basel) 13, 1125. https://doi.org/10.3390/genes13071125.

Bézivin, C., Tomasi, S., Lohézic-Le Dévéhat, F., Boustie, J., 2003. Cytotoxic activity of some lichen extracts on murine and human cancer cell lines. Phytomedicine 10, 499–503. https://doi.org/10.1078/094471103322331458.

Bojko, A., Czarnecka-Herok, J., Charzynska, A., Dabrowski, M., Sikora, E., 2019. Diversity of the Senescence Phenotype of Cancer Cells Treated with Chemotherapeutic Agents. Cells 8, 1501. https://doi.org/10.3390/cells8121501.

Brough, D., Amos, H., Turley, K., Murkin, J., 2023. Trends in Subcutaneous Tumour Height and Impact on Measurement Accuracy. Cancer Inform 22, 11769351231165181. 10.1177/11769351231165181.

Castedo, M., Perfettini, J.-L., Roumier, T., Valent, A., Raslova, H., Yakushijin, K., Horne, D., Feunteun, J., Lenoir, G., Medema, R., Vainchenker, W., Kroemer, G., 2004. Mitotic catastrophe constitutes a special case of apoptosis whose suppression entails aneuploidy. Oncogene 23, 4362–4370. https://doi.org/10.1038/sj.onc.1207572.

Chen, Q., Lesnefsky, E.J., 2006. Depletion of cardiolipin and cytochrome c during ischemia increases hydrogen peroxide production from the electron transport chain. Free. Radic. Biol. Med 40, 976–982. https://doi.org/10.1016/j.freeradbiomed.2005.10.043.

Chimplee, S., Roytrakul, S., Sukrong, S., Srisawat, T., Graidist, P., Kanokwiroon, K., 2022. Anticancer Effects and Molecular Action of 7-α-Hydroxyfrullanolide in G2/M-Phase Arrest and Apoptosis in Triple Negative Breast Cancer Cells. Molecules 27, 407. https://doi.org/10.3390/molecules27020407.

Choi, H.J., Fukui, M., Zhu, B.T., 2011. Role of Cyclin B1/Cdc2 Up-Regulation in the Development of Mitotic Prometaphase Arrest in Human Breast Cancer Cells Treated with Nocodazole. PLoS. One 6, e24312.

Cowley, D.O., Rivera-Pérez, J.A., Schliekelman, M., He, Y.J., Oliver, T.G., Lu, L., O'Quinn, R., Salmon, E.D., Magnuson, T., Van Dyke, T., 2009. Aurora-A Kinase Is Essential for Bipolar Spindle Formation and Early Development. Mol. Cell. Biol 29, 1059–1071. https://doi.org/10.1128/MCB.01062-08.

D'Angiolella, V., Santarpia, C., Grieco, D., 2007. Oxidative stress overrides the spindle checkpoint. Cell. Cycle 6, 576–579. https://doi.org/10.4161/cc.6.5.3934.

Da'i, M., Suhendi, A., Meiyanto, E., Jenie, U.A., Kawaichi, M., 2017. Apoptosis Induction Effect of Curcumin and Its Analogs Pentagamavunon-0 And Pentagamavunon-1 on Cancer Cell Lines. Asian J. Pharm. Clin. Res. 10, 373–376. 10.22159/ajpcr.2017.v10i3.16311.

Damaskos, C., Garmpi, A., Nikolettos, K., Vavourakis, M., Diamantis, E., Patsouras, A., Farmaki, P., Nonni, A., Dimitroulis, D., Mantas, D., Antoniou, E.A., Nikolettos, N., Kontzoglou, K., Garmpis, N., 2019. Triple-Negative Breast Cancer: The Progress of Targeted Therapies and Future Tendencies. Anticancer. Res 39, 5285–5296. https://doi.org/10.21873/anticanres.13722.

Darzynkiewicz, Z., Bedner, E., Traganos, F., 2001. Difficulties and pitfalls in analysis of apoptosis. Methods. Cell. Biol. 63, 527–546. https://doi.org/10.1016/s0091-679x(01)63028-0.

Davalli, P., Mitic, T., Caporali, A., Lauriola, A., D'Arca, D., 2016. ROS, Cell Senescence, and Novel Molecular Mechanisms in Aging and Age-Related Diseases. Oxid. Med. Cell. Longev 2016. https://doi.org/10.1155/2016/3565127.

Debacq-Chainiaux, F., Erusalimsky, J.D., Campisi, J., Toussaint, O., 2009. Protocols to detect senescence-associated beta-galactosidase (SA-βgal) activity, a biomarker of senescent cells in culture and in vivo. Nature. protocols 4, 1798.

Demidenko, Z.N., Kalurupalle, S., Hanko, C., Lim, C. -u, Broude, E., Blagosklonny, M.V., 2008. Mechanism of G1-like arrest by low concentrations of paclitaxel: next cell cycle p53-dependent arrest with sub G1 DNA content mediated by prolonged mitosis. Oncogene 27, 4402–4410. 10.1038/onc.2008.82.

Dong, L., Neuzil, J., 2019. Targeting mitochondria as an anticancer strategy. Cancer. Communications 39, 63. https://doi.org/10.1186/s40880-019-0412-6.

Fak, T.M., Farmasi, U.G.M., 2001. Uji Antiinflamasi Senyawa PGV-0, PGV1, dan HGV-1 Pada Tikus Jantan dan Betina dan Elusidasi Mekanisme Antiinflamasi. Fakultas Farmasi Universitas Gadjah Mada, Yogyakarta, Laporan Penelitian Tim Molnas.

Fu, J., Bian, M., Jiang, Q., Zhang, C., 2007. Roles of Aurora Kinases in Mitosis and Tumorigenesis. Mol. Cancer. Res 5, 1–10. https://doi.org/10.1158/1541-7786.MCR-06-0208.

Guerin, M.V., Finisguerra, V., Van den Eynde, B.J., Bercovici, N., Trautmann, A., 2020. Preclinical murine tumor models: A structural and functional perspective. eLife 9, e50740.

Guo, L., Kong, D., Liu, J., Zhan, L., Luo, L., Zheng, W., Zheng, Q., Chen, C., Sun, S., 2023. Breast cancer heterogeneity and its implication in personalized precision therapy. Experimental. Hematol. Oncol. 12, 3. https://doi.org/10.1186/s40164-022-00363-1.

Haschka, M., Karbon, G., Fava, L.L., Villunger, A., 2018. Perturbing mitosis for anti-cancer therapy: is cell death the only answer? EMBO Rep 19, e45440. 10.15252/embr.201745440.

Joukov, V., Nicolo, A.D., 2018. Aurora-PLK1 cascades as key signaling modules in the regulation of mitosis. Sci. Signal. 11 https://doi.org/10.1126/scisignal.aar4195.

Kamitani, N., Nakamae, I., Yoneda-Kato, N., Kato, J., Sho, M., 2022. Preclinical evaluation of pentagamavunone-1 as monotherapy and combination therapy for pancreatic cancer in multiple xenograft models. Sci. Rep 12, 22419. https://doi.org/10.1038/s41598-022-26863-y.

Kaufmann, S.H., Earnshaw, W.C., 2000. Induction of apoptosis by cancer chemotherapy. Exp. Cell. Res 256, 42–49. https://doi.org/10.1006/excr.2000.4838.

Kawamura, K., Fujikawa-Yamamoto, K., 2009. Evaluation of sub-G1 peak in mitotic catastrophe. Cytometry. Res. 19, 63–71. https://doi.org/10.18947/cytometryresearch.19.2_63.

Kumari, S., Badana, A.K., G, M.M., G, S., Malla, R., 2018. Reactive Oxygen Species: A Key Constituent in Cancer Survival. Biomark Insights 13, 1–9. 10.1177/1177271918755391.

Larasati, Y.A., Yoneda-Kato, N., Nakamae, I., Yokoyama, T., Meiyanto, E., Kato, J., 2018. Curcumin targets multiple enzymes involved in the ROS metabolic pathway to suppress tumor cell growth. Scientific. Reports 8, 2039. https://doi.org/10.1038/s41598-018-20179-6.

Lashen, A.G., Toss, M.S., Katayama, A., Gogna, R., Mongan, N.P., Rakha, E.A., 2021. Assessment of proliferation in breast cancer: cell cycle or mitosis? An observational study. Histopathology 79, 1087–1098. https://doi.org/10.1111/his.14542.

Lestari, B., Nakamae, I., Yoneda-Kato, N., Morimoto, T., Kanaya, S., Yokoyama, T., Shionyu, M., Shirai, T., Meiyanto, E., Kato, J., 2019. Pentagamavunon-1 (PGV-1) inhibits ROS metabolic enzymes and suppresses tumor cell growth by inducing M phase (prometaphase) arrest and cell senescence. Sci. Rep 9, 14867. https://doi.org/10.1038/s41598-019-51244-3.

Lindqvist, A., van Zon, W., Rosenthal, C.K., Wolthuis, R.M.F., 2007. Cyclin B1–Cdk1 Activation Continues after Centrosome Separation to Control Mitotic Progression. PLOS. Biology 5, e123.

Lovitt, C.J., Shelper, T.B., Avery, V.M., 2018. Doxorubicin resistance in breast cancer cells is mediated by extracellular matrix proteins. BMC. Cancer 18, 41. https://doi.org/10.1186/s12885-017-3953-6.

Makanjuola, D., Alkushi, A., Alzaid, M., Abukhair, O., Al Tahan, F., Alhadab, A., 2014. Breast cancer in women younger than 30 years: prevalence rate and imaging findings in a symptomatic population. Pan Afr Med J 19. 10.11604/pamj.2014.19.35.2849.

Marumoto, T., Honda, S., Hara, T., Nitta, M., Hirota, T., Kohmura, E., Saya, H., 2003. Aurora-A Kinase Maintains the Fidelity of Early and Late Mitotic Events in HeLa Cells *. J. Biol. Chem. 278, 51786–51795. https://doi.org/10.1074/jbc.M306275200.

McDermott-Lancaster, R.D., Ito, T., Kohsaka, K., Colston, M.J., 1987. The nude mouse–characteristics, breeding and husbandry. Int. J. Lepr. Other. Mycobact. Dis 55, 885–888.

Meiyanto, E., Septisetyani, E.P., Larasati, Y.A., Kawaichi, M., 2018. Curcumin Analog Pentagamavunon-1 (PGV-1) Sensitizes Widr Cells to 5-Fluorouracil through Inhibition of NF-κB Activation. Asian Pac J Cancer Prev 19, 49–56. 10.22034/APJCP.2018.19.1.49.

Meiyanto, E., Putri, H., Larasati, Y.A., Utomo, R.Y., Jenie, R.I., Ikawati, M., Lestari, B., Yoneda-Kato, N., Nakamae, I., Kawaichi, M., Kato, J., 2019. Anti-Proliferative and Anti-Metastatic Potential of Curcumin Analogue, Pentagamavunon-1 (PGV-1), Toward Highly Metastatic Breast Cancer Cells in Correlation With ROS Generation. Advanced Pharmaceutical Bulletin 9, 445–452. 10.15171/apb.2019.053.

Meiyanto, E., Husnaa, U., Kastian, R.F., Putri, H., Larasati, Y.A., Khumaira, A., Pamungkas, D.D.P., Jenie, R.I., Kawaichi, M., Lestari, B., Yokoyama, T., Kato, J.-Y., 2021. The Target Differences of Anti-Tumorigenesis Potential of Curcumin and its Analogues Against HER-2 Positive and Triple-Negative Breast Cancer Cells. Adv Pharm Bull 11, 188–196. 10.34172/apb.2021.020.

Meiyanto, E., Putri, D.D.P., Susidarti, R.A., Murwanti, R., Sardjiman, null, Fitriasari, A., Husnaa, U., Purnomo, H., Kawaichi, M.,, 2014. Curcumin and its analogues (PGV-0 and PGV-1) enhance sensitivity of resistant MCF-7 cells to doxorubicin through inhibition of HER2 and NF-kB activation. Asian. Pac. J. Cancer. Prev. 15, 179–184.

Meiyanto, E., Novitasari, D., Utomo, R.Y., Susidarti, R.A., Putri, D.D.P., Kato, J., 2022. Bioinformatic and Molecular Interaction Studies Uncover That CCA-1.1 and PGV-1 Differentially Target Mitotic Regulatory Protein and Have a Synergistic Effect against Leukemia Cells. Indonesian. J. Pharm. 33, 225–233. https://doi.org/10.22146/ijp.3382.

Moordiani, M., Novitasari, D., Susidarti, R.A., Ikawati, M., Kato, J., Meiyanto, E., 2023. Curcumin Analogs PGV-1 and CCA-1.1 Induce Cell Cycle Arrest in Human Hepatocellular Carcinoma Cells with Overexpressed MYCN. Indonesian. Biomed. J. 15, 141–149.

Novitasari, D., Jenie, R.I., Utomo, R.Y., Kato, J.Y., Meiyanto, E., 2021a. CCA-1.1, a Novel Curcumin Analog, Exerts Cytotoxic anti- Migratory Activity toward TNBC and HER2-Enriched Breast Cancer Cells. Asian Pac J Cancer Prev 22, 1827–1836. 10.31557/APJCP.2021.22.6.1827.

Novitasari, D., Meiyanto, E., Kato, J., Jenie, R.I., 2022. Antimigratory Evaluation from Curcumin-Derived Synthetic Compounds PGV-1 and CCA-1.1 on HCC1954 and MDA-MB-231 Cells. Indonesian Journal of Cancer Chemoprevention 13, 71–82. 10.14499/indonesianjcanchemoprev13iss2pp71-82.

Novitasari, D., Jenie, R.I., Wulandari, F., Putri, D.D.P., Kato, J., Meiyanto, E., 2021b. A Curcumin Like Structure (CCA-1.1) Induces Permanent Mitotic Arrest (Senescence)

on Triple Negative Breast Cancer (TNBC) Cells, 4T1. Res. J. Pharm. Technol 14, 4375–4382. https://doi.org/10.52711/0974-360X.2021.00760.
Novitasari, D., Jenie, R.I., Kato, J., Meiyanto, E., 2023a. Chemoprevention curcumin analog 1.1 promotes metaphase arrest and enhances intracellular reactive oxygen species levels on TNBC MDA-MB-231 and HER2-positive HCC1954 cells. Res. Pharm. Sci. 18, 358–370. https://doi.org/10.4103/1735-5362.378083.
Novitasari, D., Kato, J., Ikawati, M., Putri, D.D.P., Wulandari, F., Widyarini, S., Zulfin, U. M., Salsabila, D.U., Meiyanto, E., 2023b. PGV-1 permanently arrests HepG2 cells in M phase and inhibits liver carcinogenesis in DMH-induced rats. J. App. Pharm. Sci 13, 204–211. https://doi.org/10.7324/JAPS.2023.131550.
Park, J.-G., Jeon, H., Shin, S., Song, C., Lee, H., Kim, N.-K., Kim, E.E., Hwang, K.Y., Lee, B.-J., Lee, I.-G., 2023. Structural basis for CEP192-mediated regulation of centrosomal AURKA. Science Advances 9, eadf8582. 10.1126/sciadv.adf8582.
Plesca, D., Mazumder, S., Almasan, A., 2008. DNA Damage Response and Apoptosis. Methods. Enzymol 446, 107–122. https://doi.org/10.1016/S0076-6879(08)01606-6.
Reda, A., Refaat, A., Abd-Rabou, A.A., Mahmoud, A.M., Adel, M., Sabet, S., Ali, S.S., 2019. Role of mitochondria in rescuing glycolytically inhibited subpopulation of triple negative but not hormone-responsive breast cancer cells. Sci. Rep 9, 13748. https://doi.org/10.1038/s41598-019-50141-z.
Roninson, I.B., 2003. Tumor cell senescence in cancer treatment. Cancer. Res 63, 2705–2715.
Sarmoko, S., Novitasari, D., Toriyama, M., Fareza, M.S., Choironi, N.A., Itoh, H., Meiyanto, E., 2023. Different Modes of Mechanism of Gamma-Mangostin and Alpha-Mangostin to Inhibit Cell Migration of Triple-Negative Breast Cancer Cells Concerning CXCR4 Downregulation and ROS Generation. Iran. J. Pharm. Res. In. Press. https://doi.org/10.5812/ijpr-138856.
Schmucker, S., Sumara, I., 2014. Molecular dynamics of PLK1 during mitosis. Mol. Cell. Oncol 1, e954507.
Schwarze, S.R., Fu, V.X., Desotelle, J.A., Kenowski, M.L., Jarrard, D.F., 2005. The identification of senescence-specific genes during the induction of senescence in prostate cancer cells. Neoplasia 7, 816–823. https://doi.org/10.1593/neo.05250.
Shen, S.-J., Liu, C.-M., 2023. Chemotherapy for early-stage breast cancer: the more the better? The. Lancet 401, 1243–1245. https://doi.org/10.1016/S0140-6736(23)00094-6.
Starkov, A.A., 2008. The Role of Mitochondria in Reactive Oxygen Species Metabolism and Signaling. Ann. N. Y. Acad. Sci 1147, 37–52. https://doi.org/10.1196/annals.1427.015.
Sullivan, L.B., Chandel, N.S., 2014. Mitochondrial reactive oxygen species and cancer. Cancer. Metab 2, 17. https://doi.org/10.1186/2049-3002-2-17.
Tillery, M.M.L., Blake-Hedges, C., Zheng, Y., Buchwalter, R.A., Megraw, T.L., 2018. Centrosomal and Non-Centrosomal Microtubule-Organizing Centers (MTOCs) in Drosophila melanogaster. Cells 7, E121. https://doi.org/10.3390/cells7090121.
Wahler, J., Suh, N., 2015. Targeting HER2 Positive Breast Cancer with Chemopreventive Agents. Curr. Pharmacol. Rep 1, 324–335. https://doi.org/10.1007/s40495-015-0040-z.
Wang, G.-F., Dong, Q., Bai, Y., Yuan, J., Xu, Q., Cao, C., Liu, X., 2017. Oxidative stress induces mitotic arrest by inhibiting Aurora A-involved mitotic spindle formation. Free. Radical. Biology. and. Medicine 103, 177–187. https://doi.org/10.1016/j.freeradbiomed.2016.12.031.
Wanifuchi-Endo, Y., Kondo, N., Dong, Y., Fujita, T., Asano, T., Hisada, T., Uemoto, Y., Nishikawa, S., Katagiri, Y., Kato, A., Terada, M., Sugiura, H., Okuda, K., Kato, H., Takahashi, S., Toyama, T., 2022. Discovering novel mechanisms of taxane resistance in human breast cancer by whole-exome sequencing. Oncol. Lett 23, 60. https://doi.org/10.3892/ol.2021.13178.
Weerapreeyakul, N., Nonpunya, A., Barusrux, S., Thitimetharoch, T., Sripanidkulchai, B., 2012. Evaluation of the anticancer potential of six herbs against a hepatoma cell line. Chin. Med 7, 15. https://doi.org/10.1186/1749-8546-7-15.
Willmann, L., Schlimpert, M., Halbach, S., Erbes, T., Stickeler, E., Kammerer, B., 2015. Metabolic profiling of breast cancer: Differences in central metabolism between subtypes of breast cancer cell lines. J. Chromatogr. B 1000, 95–104. https://doi.org/10.1016/j.jchromb.2015.07.021.
Wu, Q., Li, Z., Huang, Y., Qian, D., Chen, M., Xiao, W., Wang, B., 2017. Oxidative stress delays prometaphase/metaphase of the first cleavage in mouse zygotes via the MAD2L1-mediated spindle assembly checkpoint. Oxidat. Med. Cell. Longevity 2017, e2103190.
Wulandari, F., Ikawati, M., Novitasari, D., Kirihata, M., Kato, J., Meiyanto, E., 2020. New curcumin analog, CCA-1.1, synergistically improves the antiproliferative effect of doxorubicin against T47D breast cancer cells. Indon. J. Pharm. 31, 244–256.
Yu, H., Yao, X., 2008. Cyclin B1: conductor of mitotic symphony orchestra. Cell. Res. 18, 218–220. https://doi.org/10.1038/cr.2008.20.